Nanoscale

Silica nanoparticle remodeling under mild conditions: versatile one step conversion of mesoporous to hollow nanoparticles with simultaneous payload loading

Journal:	*Nanoscale*
Manuscript ID	NR-COM-10-2022-005528.R1
Article Type:	Communication
Date Submitted by the Author:	15-Nov-2022
Complete List of Authors:	Shaffer, Cassandra; University of Notre Dame, Chemistry and Biochemistry Zhai, Canjia; University of Notre Dame, Chemistry and Biochemistry Chasteen, Jordan; University of Notre Dame, Chemistry and Biochemistry Orlova, Tatyana; University of Notre Dame, Notre Dame Integrated Imaging Facility Zhukovskyi, Maksym; University of Notre Dame, Notre Dame Integrated Imaging Facility Smith, B.; University of Notre Dame, Chemistry and Biochemistry

COMMUNICATION

Silica nanoparticle remodeling under mild conditions: versatile one step conversion of mesoporous to hollow nanoparticles with simultaneous payload loading†

Received 00th January 20xx,
Accepted 00th January 20xx

DOI: 10.1039/x0xx00000x

Cassandra C. Shaffer [a], Canjia Zhai [a], Jordan L. Chasteen [a], Tatyana Orlova [b], Maksym Zhukovskyi [b], and Bradley D. Smith*

A binary mixture of mesoporous silica nanoparticles plus organic polyammonium additive (dye or drug) is cleanly converted upon mild heating into hollow nanoparticles. The remodeled nanoparticle shell is an organized nanoscale assembly of globular additive/silica subunits and cancer cell assays show that a loaded drug additive is bioavailable.

Silica nanoparticles (SNPs) have been actively studied for several decades as agents for catalysis, sequestration, delivery, and imaging.[1 2 3 4] SNPs possess several attractive features such as controllable size and morphology, flexible surface modification, and biocompatibility.[5] As illustrated in Scheme 1, solid SNPs have a dense and uniform core, hollow SNPs have a shell and empty core, and mesoporous SNPs typically have narrow pores running throughout the structure. Hollow and mesoporous SNPs are usually prepared by conceptually related multistep templated synthesis processes that condense the silica matrix around an organic template (e.g., polymeric spheres in the case of hollow SNPs, or surfactant tubes in the case of mesoporous SNPs) and subsequently remove the organic templates by calcination (heating to high temperature such as 450-600 °C).[6] There are also related fabrication methods using soft and hard templates to make other types of SNP morphologies such as hollow mesoporous SNPs.[7 8 9]

Very strong silicon-oxygen bonds enable the silica framework to withstand the high temperatures used for calcination, and thermal interconversion of SNP morphology has an intrinsically high energy barrier (Scheme 1). The effect of water and metal cations on the pore-collapse temperature of mesoporous SNPs has been studied extensively, and hydrothermal stability is usually above 500 °C.[10] Nonetheless, there are reports that mesoporous SNPs degrade when dispersed in biological fluids at 37 °C.[11 12 13] The degradation mechanisms have not been investigated extensively; however, there is evidence that cationic ammonium groups promote silica hydrolysis reactions.[12 13] The SNP erosion process is usually initiated at a localized site on the particle surface and shown in Scheme 2 is a likely chemical mechanism involving electrostatic adsorption of cationic ammoniums to the anionic SNP surface followed by enhanced silica hydrolysis and release of free orthosilicic acid.[14 15 16] The SNP literature includes a couple of independent findings that added polyamines can impact silica reaction kinetics,[15 16] but there has been little work to exploit this altered surface chemistry for controlled remodeling of SNP morphology.[17 18]

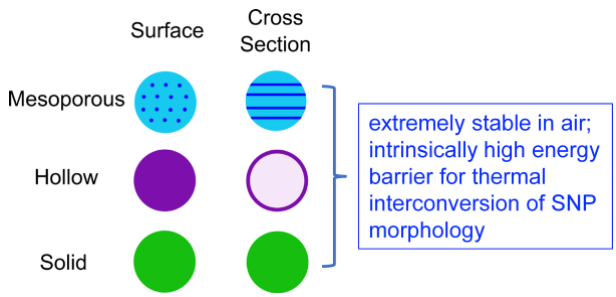

Scheme 1: Simplified diagram of different silica nanoparticle (SNP) morphologies showing views of the particle surface and cross sections.

[a] Department of Chemistry and Biochemistry, University of Notre Dame, Notre Dame, IN 46556
[b] Notre Dame Integrated Imaging Facility, University of Notre Dame, Notre Dame, IN 46556

† Electronic Supplementary Information (ESI) available: [electron microscopy images, spectral data, cell assay and microscopy results]. See DOI: 10.1039/x0xx00000x

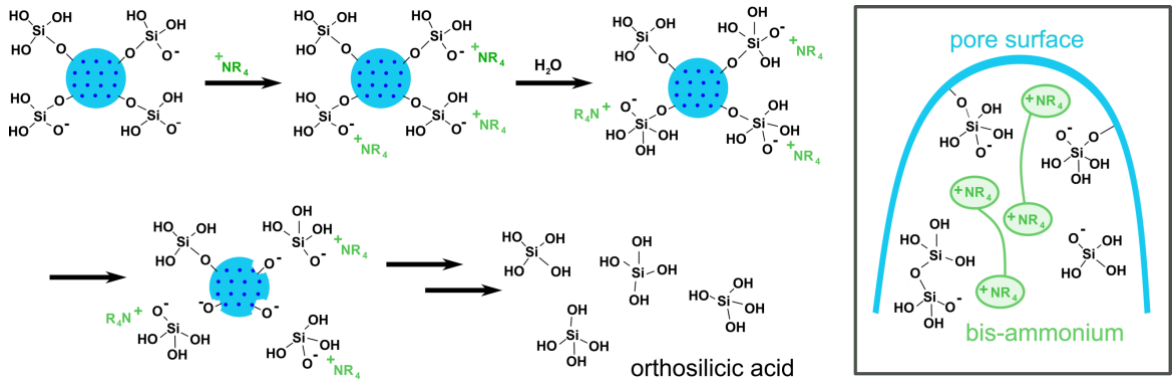

Scheme 2: Likely pathway for accelerated degradation of silica surface by ammonium cations. The boxed insert illustrates the premise that molecules containing two ammonium groups (bis-ammonium) can produce localized electrostatic effects that enhance silica hydrolysis and formation of ion pairs, with degradation of internal silica pore surfaces leading to hollow SNPs.

A corollary of the putative mechanism in Scheme 2 is that molecular additives with multiple ammonium cations can produce localized "enzyme-like" electrostatic effects that enhance silica hydrolysis, promote formation of ion pairs, and alter the nanoparticle morphology.[16 19 20] Consistent with this idea, we have discovered that organic compound containing two or more ammonium groups can be employed as additives to promote extensive remodeling of mesoporous SNPs under mild conditions. Specifically, we have developed a one step process that converts commercially available mesoporous SNPs into hollow structures (Scheme 3). The bis-ammonium compounds, *p*-xylylenediamine and mitoxantrone, are exemplary chemical additives and they were used to remodel commercial mesoporous nanoparticles (100 nm particle diameter, 3.74 nm pore diameter). A typical procedure mixed a solution of bis-ammonium compound (0.4 mg in 50 µL DMSO)‡ with a dispersion of mesoporous nanoparticles (1 mg in 3 mL phosphate buffered saline, PBS, pH 7.4) in a 50 mL centrifuge tube. The sample was heated overnight at 75-80 °C with exposure to air, then allowed to stir for an additional day at room temperature. The dispersion was centrifuged, the solvent removed, and the pellet containing the nanoparticles was cleaned with three cycles of washing/centrifugation/redispersion using distilled water (5 mL) before being brought to a final SNP concentration of 1 mg/mL in H_2O.

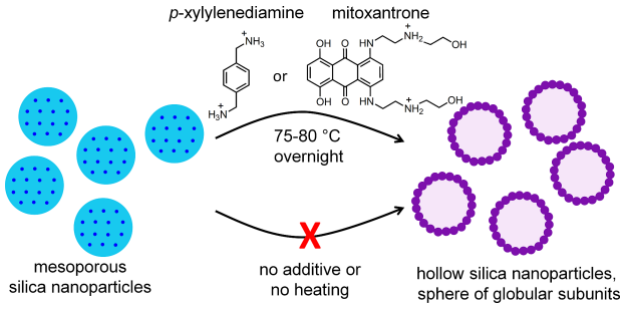

Scheme 3: Bis-ammonium compounds (*p*-xylylenediamine or mitoxantrone) are exemplary additives that convert mesoporous SNPs into hollow SNPs with mild heating.

TEM (Transmission Electron Microscopy) and SEM (Scanning Electron Microscopy) methods were employed extensively in this project and the images of untreated commercial mesoporous SNPs in Figure 1a and Figures S1-S2 confirm the uniform size (100 nm diameter) and internal network of 3.74 nm pores. Simply heating these mesoporous nanoparticles at 75-80 °C without any chemical additive causes partial degradation of the nanoparticle structure but does not form hollow SNPs (see representative TEM images in Figure 1b and Figures S3). But when the mesoporous SNPs were heated in the presence of *p*-xylylenediamine, a very large fraction of the nanoparticles were converted to hollow SNPs, as shown by the representative TEM images in Figures 1c and S4. Inspection of multiple TEM images from independent replicate experiments indicated a reproducible process that produced hollow SNPs with a diameter ~100 nm and shell thickness of 5-8 nm. The SEM imaging provided significant additional insight concerning the hollow SNP morphology (Figures 1d and S5-S6). Specifically, the shell of each hollow SNP is an organized spherical assembly of globular subunits with an occasional shell opening that reveals the hollow core. There are literature reports of similar hollow SNP morphologies (called virus-like,[21] raspberry-like,[22] colloidalsomes[23] or hollow nanospheres[24]) but they were obtained using more complicated, templated fabrication methods. Control experiments showed that the hollow SNPs were not formed if there was; (a) no heating of the binary mixture containing mesoporous SNPs and polyammonium (Figure S7) which is consistent with literature observations,[25 26] (b) solid silica nanoparticles were used in place of mesoporous SNPs (Figure S8), or (c) benzylamine (one ammonium group) was used in place of *p*-xylylenediamine (two ammonium groups) (Figure S9). The latter result agrees with reports that simple organic additives (including monoamines) only induce mesoporous SNPs to undergo pore swelling.[18]

We hypothesized that the bis-ammonium additive (*p*-xylylenediamine) remodeled the mesoporous SNPs by promoting degradation reactions at the internal silica pore surfaces leading to formation of small, non-covalently linked additive/silica subunits (see boxed insert in Scheme 2). [16 19 20 27] Support for this idea was gained by conducting a systematic

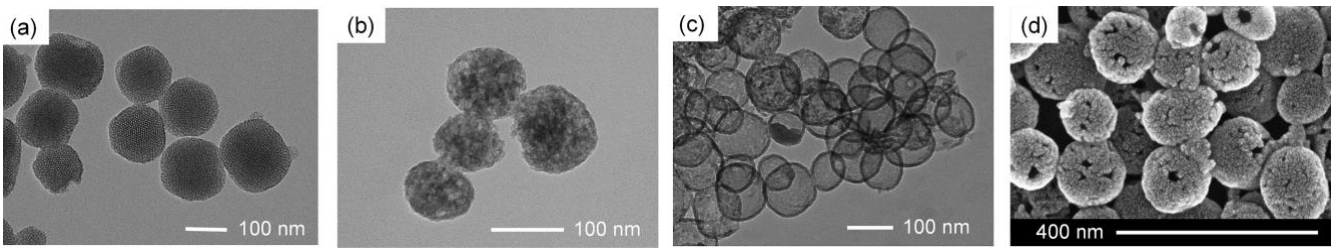

Figure 1: Representative TEM images of, (a) untreated mesoporous SNPs (100 nm particle diameter, 3.74 nm pore diameter) in PBS before heating, and (b) partially degraded mesoporous SNPs after heating in PBS overnight at 75-80 °C. Representative TEM (c) and SEM (d) images of hollow SNPs created by heating mesoporous SNPs plus *p*-xylylenediamine

series of control studies that heated separate mixtures of mesoporous SNPs with three different but structurally related squaraine dyes that were available in our lab from previous studies.[28 29] These deep-red dyes were chosen, in part, because they survive overnight heating in PBS and because they exhibit very similar spectral properties but differ in the number of ammonium groups (dye structures are provided in the ESI). As shown by the representative TEM images in Figures S10-S11, the presence of dye **S2** (two ammonium groups) or dye **S4** (four ammonium groups) produced hollow SNPs. In contrast, the presence of dye **S0** (zero ammonium groups) did not produce hollow SNPs (Figure S12). The absorption spectra of washed samples of hollow SNPs formed by heating mesoporous SNPs with dye **S4** revealed a characteristic deep-red maxima peak, indicating the squaraine dye was physically incorporated within the structure of the hollow SNP (Figure S20).

A similar remodeling outcome was obtained when we employed the drug mitoxantrone as the bis-ammonium additive. As indicated by the TEM and SEM images in Figure 2a-b and Figures S13-S14, heating a binary mixture of mesoporous SNPs and mitoxantrone in PBS produced a mixture of predominantly hollow SNPs with a small fraction of unchanged mesoporous SNPs. SEM and Scanning Transmission Electron Microscopy (STEM) imaging of these samples (Figures S15-S16) highlighted the significant morphological difference between the mesoporous SNPs and the hollow SNPs, and this difference was confirmed with Energy-Dispersive X-ray (EDX) analysis of the samples (Figure S17). A clear visual illustration of this difference is gained by inspecting the STEM image in Figure 2c and the corresponding EDX map of nitrogen atoms in the same image (Figure 2d). Since mitoxantrone is the only source of nitrogen atoms in the sample, it is apparent that the drug is distributed uniformly throughout the two mesoporous SNPs within the image but localizes only in the shells of the hollow SNPs.[§] A final synthetic point with the hollow SNPs produced by heating mesoporous SNPs with mitoxantrone is the possibility of fine-tuning the nanoparticle dimensions. Specifically, we evaluated the effect of a longer heating period, and found that heating for 48 hours produced hollow SNPs with significantly thicker 20-30 nm shells (Figure S19) along with some particle degradation. Thus, it is feasible to systematically modify the reaction conditions to produce SNPs with customized silica/payload composition and precise morphologies such as a specifically desired hollow nanoparticle diameter or shell thickness. [19 20 27]

Mitoxantrone is a type II topoisomerase inhibitor, and it is used clinically to treat certain types of cancer and multiple sclerosis.[30] The risk of cardiomyopathy has motivated efforts to develop nanoparticle versions of mitoxantrone for controlled release, and there are published studies of mesoporous SNPs loaded with mitoxantrone (mitoxantrone@mesoporousSNP).[31 32] There are also reports of mitoxantrone-loaded nanoparticles for selective delivery to solid tumors.[33 34] In this cancer treatment context, we envision mitoxantrone@hollowSNP as a potential two step drug delivery platform that exploits the enhanced permeability and retention (EPR) effect for initial accumulation of the 100 nm mitoxantrone@hollowSNP within tumors,[33 34] followed by diffusion of smaller mitoxantrone/silica subunits that fragment from the nanoparticle and permeate into restricted cancer cell locations within the tumor

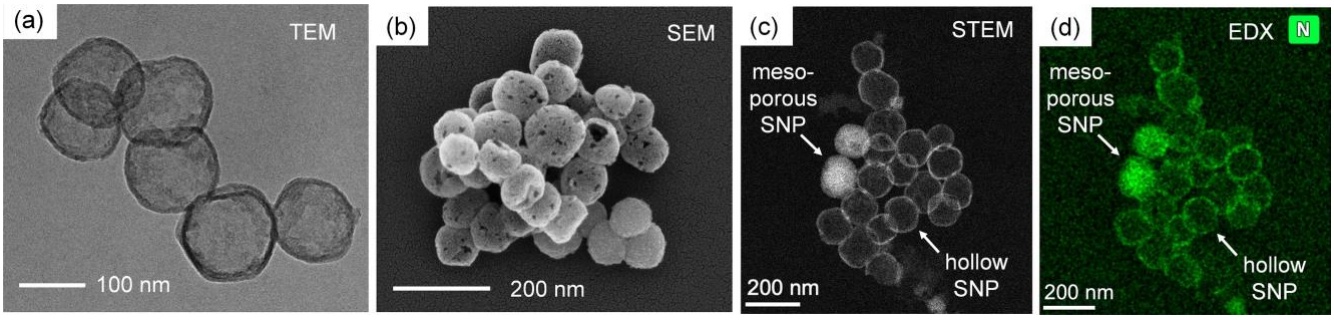

Figure 2: Representative TEM (a) and SEM (b) images of hollow SNPs created by heating mesoporous SNPs plus mitoxantrone in PBS at 75-80 °C. STEM image (c) of a sample comprised of hollow SNPs and two unconverted mesoporous SNPs; the sample was created by heating mesoporous SNPs plus mitoxantrone in PBS at 75-80 °C; (d) EDX map of nitrogen atoms in the same image.

microenvironment.[35 36] Since mitoxantrone is a red-absorbing drug molecule, it was straightforward to measure drug loading into the SNPs using absorption spectroscopy.[37] As summarized in the ESI, the drug loading efficiency was determined to be 87% for creation of mitoxantrone@mesoporousSNP at room temperature and 67% for creation of mitoxantrone@hollowSNP produced by overnight heating at 75-80 °C. To determine if the entrapped mitoxantrone was still pharmaceutically active, we conducted a series of cell metabolic assays using cultures of A549 (human lung adenocarcinoma) and MCF-7 (human breast adenocarcinoma) cells. A standard MTT assay was employed and IC_{50} values were determined for three formulations, (a) free mitoxantrone, (b) mitoxantrone that has been loaded into mesoporous SNPs (mitoxantrone@mesoporousSNP), and (c) mitoxantrone used to create hollow SNPs (mitoxantrone@hollowSNP).[37] As summarized in Table 1 and Figure S21, measured IC_{50} values were in the submicromolar range for all three mitoxantrone formulations in both cell lines, consistent with literature values.[37 38] We conclude that the mitoxantrone chemical structure in each formulation is not degraded by the SNP loading procedure and that after introduction to the cell culture, the active drug can escape the SNP and reach its intracellular enzyme target.[§§] It is worth noting that a wide range of pharmaceuticals and biologically active compounds have two or more ammonium groups,[39 40 41 42] and that the US Food and Drug Administration (FDA) classifies silica as a substance that is "generally recognized as safe".[36 43] Thus, our one step method for SNP remodeling and drug loading has potential to become a general drug@hollowSNP formulation to treat different diseases, with the minor caveat that the pharmaceutically active ingredient must survive the overnight heating at 75-80 °C required for drug@hollowSNP fabrication.

In summary, we report a simple and versatile new method for converting commercially available mesoporous SNPs into hollow SNPs with simultaneous loading of a chemical additive that contains two or more cationic ammonium groups. The proof of concept experiments in this study created dye@hollowSNP and drug@hollowSNP formulations for potential applications in drug delivery and optical imaging, with an implication that the method can be used to incorporate other types of useful amine-containing molecular payload such as catalysts,[44] absorbents,[45 46] and release agents.[47] The discovery suggests a new mechanism-based paradigm for predictable mesoporous silica nanoparticle remodeling under mild conditions using judiciously designed polyammonium compounds.[14 16 18 19 20 48 49] The conceptual strategy of using organic polyammonium compounds to remodel inorganic silica matrices is reminiscent of natural biomineralization processes deployed by organisms such as diatoms.[48] Better mimics of these biomineralization processes will facilitate long term efforts to rationally design new classes of hybrid organic/inorganic materials.[48 50 51 52 53 54]

Table 1. IC_{50} Values (μM).[a]

	MCF-7 cells	A549 cells
free mitoxantrone	0.4 ± 0.2	0.2 ± 0.1
mitoxantrone@mesoporousSNP	0.3 ± 0.2	0.2 ± 0.1
mitoxantrone@hollowSNP	0.3 ± 0.1	0.5 ± 0.2

[a]Average and standard deviation of triplicate measurements.

Conflicts of interest

There are no conflicts to declare.

Acknowledgements

We are grateful for funding support from the US NSF (CHE 2103598), and NIH ((R35GM136212 and T32GM075762).

Notes and references

‡ Control experiments that omitted the DMSO still produced the same amounts of hollow SNPs, see Figure S14.

§ EDX analysis of untreated mesoporous SNPs produced no measurable nitrogen signal indicating an absence of nitrogen containing impurities such as the surfactant CTAB (see Figure S18).

§§ Described in section 4 of the ESI is a set of confocal microscopy studies that imaged cancer cells after they were treated with fluorescent dye **S4** or **S4**@hollowSNP and observed a large difference in the intracellular location. This shows that a major change in cell localization can be produced by simply formulating a suitable payload molecule as a hollow SNP. A goal of future studies is to elucidate the underlying cell uptake and payload release mechanisms.

1 V. Gubala, G. Giovannini, F. Kunc, M. P. Monopoli and C. J. Moore, *Cancer Nanotechnol.*, 2020, **11**, 1–43.
2 D. Yuan, C. M. Ellis and J. J. Davis, *Materials*, 2020, **13**, 16–18.
3 A. N. Frickenstein, J. M. Hagood, C. N. Britten, B. S. Abbott, M. W. McNally, C. A. Vopat, E. G. Patterson, W. M. Maccuaig, A. Jain, K. B. Walters and L. R. McNally, *Pharmaceutics*, 2021, **13**, 1–27.
4 M. Vallet-Regí, F. Schüth, D. Lozano, M. Colilla and M. Manzano, *Chem. Soc. Rev.*, 2022, **51**, 5356-545.
5 V. Bueno and S. Ghoshal, *Langmuir*, 2020, **36**, 14633–14643.
6 P. Singh, S. Srivastava and S. K. Singh, *ACS Biomater. Sci. Eng.*, 2019, **5**, 4882–4898.
7 W. Chen, C. A. Cheng, E. D. Cosco, S. Ramakrishnan, J. G. P. Lingg, O. T. Bruns, J. I. Zink and E. M. Sletten, *J. Am. Chem. Soc.*, 2019, **141**, 12475–12480.
8 R. Narayan, U. Y. Nayak, A. M. Raichur and S. Garg, *Pharmaceutics*, 2018, **10**, 1–49.
9 Z. Teng, W. Li, Y. Tang, A. Elzatahry, G. Lu and D. Zhao, *Adv. Mater.*, 2019, **31**, 1–24.

10 S. C. Shen and S. Kawi, *J. Phys. Chem. B*, 1999, **103**, 8870–8876.
11 Y. S. Lin, N. Abadeer and C. L. Haynes, *Chem. Commun.*, 2011, **47**, 532–534.
12 S. P. Hadipour Moghaddam, R. Mohammadpour and H. Ghandehari, *J. Control. Release*, 2019, **311**–**312**, 1–15.
13 A. da Cruz Schneid, L. J. C. Albuquerque, G. B. Mondo, M. Ceolin, A. S. Picco and M. B. Cardoso, *J. Sol-Gel Sci. Technol.*, 2022, **102**, 41–62.
14 S. A. Yang, S. Choi, S. M. Jeon and J. Yu, *Sci. Rep.*, 2018, **8**, 1–9.
15 E. Neofotistou and K. D. Demadis, *Colloids Surfaces A Physicochem. Eng. Asp.*, 2004, **242**, 213–216.
16 G. Della Rosa, R. Di Corato, S. Carpi, B. Polini, A. Taurino, L. Tedeschi, P. Nieri, R. Rinaldi and A. Aloisi, *Sci. Rep.*, 2020, **10**, 1–15.
17 A. Rodríguez-Ramos, L. Marín-Caba, N. Iturrioz-Rodríguez, E. Padín-González, L. García-Hevia, T. M. Oliveira, M. A. Corea-Duarte and M. L. Fanarraga, *Int. J. Mol. Sci.*, 2020, **21**, 1–13.
18 K. Möller and T. Bein, *Chem. Mater.*, 2017, **29**, 371–388.
19 E. Brunner, K. Lutz and M. Sumper, *Phys. Chem. Chem. Phys.*, 2004, **6**, 854–857.
20 S. P. Maddala, W. C. Liao, R. R. M. Joosten, M. Soleimani, R. Tuinier, H. Friedrich and R. A. T. M. van Benthem, *Commun. Chem.*, 2021, **4**, 1–11.
21 D. Xu, X. Song, J. Zhou, X. Ouyang, J. Li and D. Deng, *Colloids Surfaces B Biointerfaces*, 2021, **197**, 111452.
22 C. Wang, J. Yan, Z. Li, H. Wang and X. Cui, *J. Nanopart. Res.*, 2013, **15**, 1937.
23 H. Wang, X. Zhu, L. Tsarkova, A. Pich and M. Möller, *ACS Nano*, 2011, **5**, 3937–3942.
24 J. Park, D. A. Cullen, J. Chen, G. Polizos and J. Sharma, *Appl. Surf. Sci.*, 2019, **467**–**468**, 634–639.
25 B. González, M. Colilla, J. Díez, D. Pedraza, M. Guembe, I. Izquierdo-Barba and M. Vallet-Regí, *Acta Biomater.*, 2018, **68**, 261–271.
26 S. Kachbouri, N. Mnasri, E. Elaloui and Y. Moussaoui, *J. Saudi Chem. Soc.*, 2018, **22**, 405–415.
27 H. L. Swanson, C. Guo, M. Cao, J. B. Addison and G. P. Holland, *Phys. Chem. Chem. Phys.*, 2020, **22**, 20349–20361.
28 C. Zhai, C. L. Schreiber, S. Padilla-Coley, A. G. Oliver and B. D. Smith, *Angew. Chem. Int. Ed.*, 2020, **59**, 23740–23747.
29 S. Xiao, N. Fu, K. Peckham and B. D. Smith, *Org. Lett.*, 2010, **12**, 140–143.
30 B. J. Evison, B. E. Sleebs, K. G. Watson, D. R. Phillips and S. M. Cutts, *Med. Res. Rev.*, 2016, **36**, 248–299.
31 A. Wani, E. Muthuswamy, G. H. L. Savithra, G. Mao, S. Brock and D. Oupický, *Pharm. Res.*, 2012, **29**, 2407–2418.
32 A. Wani, G. H. L. Savithra, A. Abyad, S. Kanvinde, J. Li, S. Brock and D. Oupický, *Sci. Rep.*, 2017, **7**, 1–11.
33 R. D. Lin and N. F. Steinmetz, *Nanoscale*, 2018, **10**, 16307–16313.
34 C. L. Li, J. X. Cui, C. X. Wang, Y. G. Li, H. W. Zhang, J. X. Wang, Y. H. Li, L. Zhang, L. Zhang, W. M. Guo and Y. L. Wang, *Eur. J. Pharm. Biopharm.*, 2008, **70**, 657–665.
35 Y. Nakamura, A. Mochida, P. L. Choyke and H. Kobayashi, *Bioconjug. Chem.*, 2016, **27**, 2225–2238.
36 M. Gisbert-Garzarán and M. Vallet-Regí, *Nanomaterials*, 2020, **10**, 916.
37 S. Grund, T. Doussineau, D. Fischer and G. J. Mohr, *J. Colloid Interface Sci.*, 2012, **365**, 33–40.
38 Y. Ma, L. Zhou, H. Zheng, L. Xing, C. Li, J. Cui and S. Che, *J. Mater. Chem.*, 2011, **21**, 9483–9486.
39 M. P. Mingeot-Leclercq, Y. Glupczynski and P. M. Tulkens, *Antimicrob. Agents Chemother.*, 1999, **43**, 727–737.
40 M. D. T. Senanayake, H. Amunugama, T. D. Boncher, R. A. Casero and P. M. Woster, *Essays Biochem.*, 2009, **46**, 77–94.
41 T. Hussain, B. Tan, W. Ren, N. Rahu, R. Dad, D. H. Kalhoro and Y. Yin, *Amino Acids*, 2017, **49**, 1457–1468.
42 S. Nakanishi and J. L. Cleveland, *Med. Sci.*, 2021, **9**, 28.
43 J. Y. Liu and C. M. Sayes, *Toxicol. Res.*, 2022, **11**, 565–582.
44 P. S. Shinde, P. S. Suryawanshi, K. K. Patil, V. M. Belekar, S. A. Sankpal, S. D. Delekar and S. A. Jadhav, *J. Compos. Sci.*, 2021, **5**, 1–17.
45 Y. Fan and X. Jia, *Energy and Fuels*, 2022, **36**, 1252–1270.
46 W. Naowanon, R. Chueachot, S. Klinsrisuk and S. Amnuaypanich, *Powder Technol.*, 2018, **323**, 548–557.
47 J. C. S. Terra, A. Moores and F. C. C. Moura, *ACS Sustain. Chem. Eng.*, 2019, **7**, 8696–8705.
48 H. Zhai, T. Bendikov and A. Gal, *Angew. Chem. Int. Ed.*, 2022, **17**, e202115930
49 C. Y. Lin, C. M. Yang and M. Lindén, *J. Colloid Inter. Sci.*, 2022, **608**, 995–1004.
50 Y. Chen, Y. Feng, J. G. Deveaux, M. A. Masoud, F. S. Chandra, H. Chen, D. Zhang and L. Feng, *Minerals*, 2019, **9**, 1–21.
51 Z. H. Nie, Y. Q. Zhang, R. K. Tang and X. Y. Wang, *J. Inorg. Biochem.*, 2022, **232**, 111815.
52 J. J. Xie, H. Ping, T. N. Tan, L. W. Lei, H. Xie, X. Y. Yang and Z. Y. Fu, *Prog. Mater. Sci.*, 2019, **105**, 100571.
53 J. R. H. Manning, C. Brambila and S. V. Patwardhan, *Mol. Syst. Des. Eng*., 2021, **6**, 170–196.
54 D. J. Belton, O. Deschaume and C. C. Perry, *FEBS J.*, 2012, **279**, 1710–1720.